CHEMISTRY OF
MATERIALS
Article

DOI:10.1021/cm1025848

Nanocrystalline Cerium−Bismuth Oxides: Synthesis, Structural Characterization, and Redox Properties

Kripasindhu Sardar,[†] Helen Y. Playford,[†] Richard J. Darton,[†,‡] Emma R. Barney,[§]
Alex C. Hannon,[§] David Tompsett,[‖] Janet Fisher,[‖] Reza J. Kashtiban,[⊥] Jeremy Sloan,[⊥]
Silvia Ramos,[⊗] Giannantonio Cibin,[⊗] and Richard I. Walton*,[†]

[†]*Department of Chemistry, University of Warwick, Coventry, CV4 7AL, U.K.,* [§]*ISIS Facility, Rutherford Appleton Laboratory, Harwell Science and Innovation Campus, Didcot, OX11 0QX, U.K.,* [‖]*Johnson Matthey Technology Centre, Sonning Common, Reading, RG4 9NH, U.K.,* [⊥]*Department of Physics, University of Warwick, Coventry, CV4 7AL, U.K., and* [⊗]*Diamond Light Source, Harwell Science and Innovation Campus, Didcot, OX11 0DE, U.K.* [‡]*Current address: School of Physical & Geographical Sciences, Keele University, Staffordshire, ST5 5BG, U.K.*

Received September 9, 2010. Revised Manuscript Received October 14, 2010

The hydrothermal oxidation of Ce^{3+} in basic aqueous solution by $NaBi^{V}O_3$ at 240 °C produces fine powders of cerium−bismuth oxides with crystallite sizes of less than 10 nm, as observed by transmission electron microscopy (TEM). Analysis of X-ray absorption near-edge structure at the Bi L_{III} and Ce L_{III} edges confirms the reduction of Bi^{5+} to Bi^{3+} and the oxidation of Ce^{3+} to Ce^{4+}, consistent with a general chemical composition $Ce^{IV}{}_{1-x}Bi^{III}{}_{x}O_{2-(x/2)}$ ($x \leq 0.6$) for the mixed oxides. The refined cubic lattice parameters from powder neutron diffraction indicate a fluorite-like solid solution with volume that increases with Bi content. Pair distribution functions derived from total neutron scattering yield estimated values for refined particle diameters that agree with TEM, showing a decreasing crystallite diameter with increasing bismuth content, and a full analysis reveals that despite average long-range structure being described well as a fluorite solid-solution, the local structure is distorted. Thus, the short-range structure can be simulated as a mixture of symmetric eight-coordinate Ce sites, as seen in CeO_2, and distorted Bi sites, as seen in β-Bi_2O_3. Temperature programmed reduction studies reveal a large hydrogen uptake in the mixed oxides, which is reproducible on a second subsequent cycle. *In situ* powder XRD under hydrogen flow, however, reveals that this is due to partial phase separation to give bismuth metal. After six cycles, a material of initial composition $Ce_{0.5}Bi_{0.5}O_{1.75}$ is completely phase-separated and its hydrogen uptake is reduced with high-resolution TEM analysis confirming the permanent reduction of the sample.

Introduction

Ceria, CeO_2, forms an active component of some important catalysts[1] in applications including automotive three-way catalytic converters,[2] electrodes in solid-oxide fuels cells,[3] in water gas shift for the production and purification of hydrogen from water and carbon monoxide,[4] and in selective catalytic oxidations of, for example, hydrocarbons or small inorganic molecules.[5] In these situations, ceria is often used as a redox-active solid support for precious metals where it plays the role of an oxygen-level buffer due to its oxygen storage capacity, a property associated with considerable oxide ion mobility in the solid-state and the ability of cerium to interconvert rapidly and reversibly between the 4+ and 3+ oxidation states at moderate temperatures. This may be ascribed to the fluorite structure it adopts, an open oxide structure associated with oxygen migration.[6] Doping of ceria by a range of substituent metals has been investigated as a means of tuning the oxygen storage, oxide-ion conductivity, and redox properties of the material. Dopant cations range from isovalent Zr^{4+}[7,8] and Sn^{4+},[9] aliovalent ions such as Y^{3+}, Gd^{3+}, Sm^{3+}, and Sr^{2+} whose lower charge introduces compensating oxide ion vacancies thus potentially enhancing oxide-ion migration activity,[10] to

---

(1) Trovarelli, A.; de Leitenburg, C.; Boaro, M.; Dolcetti, G. *Catal. Today* **1999**, *50*, 353. *Catalysis by Ceria and Related Materials*; Trovarelli, A., Ed.; Imperial College Press: London, 2002.

(2) Kašpar, J.; Fornasiero, P.; Graziani, M. *Catal. Today* **1999**, *50*, 285.

(3) Lashtaberg, A.; Skinner, S. J. *J. Mater. Chem.* **2006**, *16*, 3161.

(4) Kušar, H.; Hočevar, S.; Levec, J. *Appl. Catal., B: Environ.* **2006**, *63*, 194.

(5) Beckers, J.; Rothenberg, G. *Green Chem.* **2010**, *12*, 939.

(6) Giordano, F.; Trovarelli, A.; de Leitenburg, C.; Giona, M. *J. Catal.* **2000**, *193*, 273.

(7) Monte, R. D.; Kašpar, J. *Catal. Today* **2005**, *100*, 27. Monte, R. D.; Kašpar, J. *J. Mater. Chem.* **2005**, *15*, 633.

(8) Baidya, T.; Hegde, M. S.; Gopalakrishnan, J. *J. Phys. Chem. B* **2007**, *111*, 5149.

(9) Sasikala, R.; Gupta, N. M.; Kulshreshtha, S. K. *Catal. Lett.* **2001**, *71*, 69. Baidya, T.; Gupta, A.; Deshpandey, P. A.; Madras, G.; Hegde, M. S. *J. Phys. Chem. C* **2009**, *113*, 4059. Gupta, A.; Hegde, M. S.; Priolkar, K. R.; Waghmare, U. V.; Sarode, P. R.; Emura, S. *Chem. Mater.* **2009**, *21*, 5836.

(10) Wang, D. Y.; Park, D. S.; Griffith, J.; Nowick, A. S. *Solid State Ionics* **1981**, *2*, 95. Balazs, G. B.; Glass, R. S. *Solid State Ionics* **1995**, *76*, 155. Yamashita, K.; Ramanujachary, K. V.; Greenblatt, M. *Solid State Ionics* **1995**, *81*, 53.

transition-metal cations such as Ti^{4+},[11] Cu^{2+},[4] Fe^{3+},[12] and Pd^{2+},[13] which themselves might show redox activity. In addition to their catalytic activity, ceria and its doped analogues also find use in other areas including UV-shielding,[14] as abrasive agents for chemical mechanical planarization of integrated circuits,[15] and as humidity sensors.[16]

Bismuth-doped ceria has already been studied by a number of researchers, since as well as introducing oxide-ion vacancies to balance charge, the unsymmetrical coordination environment preferred by Bi^{3+} with its $6s^2$ pair of valence electrons may introduce extra structural distortion, advantageous for oxide-ion migration. For example, Dikmen et al. found high oxide ion conductivity in small particles that could be sintered at lower temperatures than conventional ceramics when hydrothermal synthesis was used for the preparation of Bi-doped CeO_2.[17] Li et al. studied nanocrystalline $Ce_{1-x}Bi_xO_y$ ($0.1 < x < 0.5$) for its ionic conductivity.[18] Zhao and Feng introduced greater complexity by codoping with Bi^{3+} and M^{2+} (M = Ca, Sr, Ba) and found that the choice of Bi source is crucial for the preparation of phase pure samples but that the resulting materials show high levels of oxide-ion conductivity, found to be optimal for the phase $Ce_{0.95}Ca_{0.05}Bi_{0.4}O_{2.55}$.[19] The same group also prepared nanocrystalline samples that showed favorable sintering properties into ceramic pellets.[20] Recently, Beckers et al. have reported that ceria doped with 10% bismuth is a highly active and selective oxidation catalyst for hydrogen combustion.[21]

Although Bi-doped ceria materials have been shown to have favorable properties for various applications, their structures have not generally been investigated in great detail and this has been complicated by the nanocrystalline nature of samples prepared using soft chemical processes, which makes full analysis of Bragg diffraction data problematic. Arguably the most detailed study of such materials is contained in a brief conference report by Frolova et al. who used a combination of EXAFS and high energy X-ray scattering to examine radial distribution of local structure in some representative cerium-bismuth oxides,[22] although the results obtained were rather qualitative since no fitting to the data was actually performed. In this paper we describe a full structural characterization of fluorite-like cerium–bismuth oxides prepared by a new synthetic route involving the Bi(V) containing precursor $NaBiO_3 \cdot nH_2O$ ($n \sim 2$) as an oxidant under hydrothermal conditions. This reagent has previously been used by Kumada and co-workers to prepare a variety of binary and mixed-metal bismuth-containing oxides directly from solution under hydrothermal conditions.[23,24] In the case of cerium oxides, we have now found $NaBiO_3 \cdot nH_2O$ to provide a convenient one-step route to Bi-doped ceria in a nanocrystalline form, whose structure we have investigated using total neutron scattering and whose redox properties we have also investigated, focusing on the standard method of temperature programmed reduction for comparison with other reported ceria-based materials.

Experimental Section

Samples of cerium–bismuth oxides were prepared by hydrothermal synthesis from metal salts in aqueous basic solution using Teflon-lined, stainless-steel autoclaves. The level of hydration of the metal salts was determined using thermogravimetric analysis. In a typical synthesis, $NaBiO_3 \cdot 2H_2O$ (85% Acros Organics) and $CeCl_3 \cdot 7H_2O$ (99.9% Alfa Aesar) with desired stoichiometric ratio (based on 2–3 mmol of $NaBiO_3 \cdot 2H_2O$) were stirred in 4 mL of 4 M HNO_3 solution for 10 min, to which 4 mL of 10 M NaOH was added dropwise with stirring for another 25 min. The reaction mixtures were sealed in autoclaves and then placed in a preheated fan oven at 240 °C for 96 h, before cooling to room temperature. After the reaction, an orange-yellow precipitate was obtained which was recovered by suction filtration. All the solid products were washed with hot water and dried at 100 °C for a few hours before further characterization. Elemental analysis for metals was performed using ICP-MES for Ce, Bi, and Na (by Medac Ltd. U.K.).

Powder XRD data were collected using Bruker D8 Advance X-ray diffractometer operating with Cu Kα radiation and equipped with a VÅNTEC-1 solid-state detector. The diffractometer was fitted with an Anton-Parr XRK900 chemical reaction chamber to allow measurements to be made as a function of temperature and gas environment. As will be described below, *in situ* diffraction studies under reducing conditions were performed: here the powder sample was exposed to a continuous flow (1–2 bar) of dry 5% H_2 in N_2. After flushing the cell to remove air, the sample was heated with a typical rate of 2 °C min^{-1} and diffraction data recorded at chosen, fixed temperatures

---

(11) Baidya, T.; Gayen, A.; Hegde, M. S.; Ravishankar, N.; Dupont, L. *J. Phys. Chem. B* **2006**, *110*, 5262. Dutta, G.; Waghmare, U. V.; Baidya, T.; Hegde, M. S.; Priolkar, K. R.; Sarode, P. R. *Chem. Mater.* **2006**, *18*, 3249.

(12) Li, G.; Smith, R. L.; Inomata, H. *J. Am. Chem. Soc.* **2001**, *123*, 11091.

(13) Roy, S.; Hegde, M. S. *Catal. Commun.* **2008**, *9*, 811.

(14) Yabe, S.; Yamashita, M.; Momose, S.; Tahira, K.; Yoshida, S.; Li, R. X.; Yin, S.; Sato, T. *Int. J. Inorg. Mater.* **2001**, *3*, 1003. Yabe, S.; Sato, T. *J. Solid State Chem.* **2003**, *171*, 7.

(15) Feng, X. D.; Sayle, D. C.; Wang, Z. L.; Paras, M. S.; Santora, B.; Sutorik, A. C.; Sayle, T. X. T.; Yang, Y.; Ding, Y.; Wang, X. D.; Her, Y. S. *Science* **2006**, *312*, 1504.

(16) Fu, X. Q.; Wang, C.; Yu, H. C.; Wang, Y. G.; Wang, T. H. *Nanotechnology* **2007**, *18*, 145503.

(17) Dikmen, S.; Shuk, P.; Greenblatt, M. *Solid State Ionics* **1998**, *112*, 299.

(18) Li, G. S.; Mao, Y. C.; Li, L. P.; Feng, S. H.; Wang, M. Q.; Yao, X. *Chem. Mater.* **1999**, *11*, 1259.

(19) Zhao, H.; Feng, S. H. *Chem. Mater.* **1999**, *11*, 958.

(20) Zhao, H.; Feng, S.; Xu, W. *Mater. Res. Bull.* **2000**, *35*, 2379.

(21) Beckers, J.; Lee, A. F.; Rothenberg, G. *Adv. Synth. Catal.* **2009**, *351*, 1557.

(22) Frolova, Y. V.; Kochubey, D. I.; Kriventsov, V. V.; Moroz, E. M.; Neofitides, S.; Sadykov, V. A.; Zyuzin, D. A. *Nucl. Instrum. Methods Phys. Res., Sect. A* **2005**, *543*, 127.

(23) Kumada, N.; Hosoda, M.; Kinomura, N. *J. Solid State Chem.* **1993**, *106*, 476. Kodialam, S.; Kumada, N.; Mackay, R.; Sleight, A. W. *Eur. J. Solid State Inorg. Chem.* **1994**, *31*, 739. Kumada, N.; Kinomura, N.; Kodialam, S.; Sleight, A. W. *Mater. Res. Bull.* **1994**, *29*, 497. Kumada, N.; Takahashi, N.; Kinomura, N.; Sleight, A. W. *J. Solid State Chem.* **1996**, *126*, 121. Kumada, N.; Takahashi, N.; Kinomura, N.; Sleight, A. W. *Mater. Res. Bull.* **1997**, *32*, 1003. Kumada, N.; Takahashi, N.; Kinomura, N.; Sleight, A. W. *J. Solid State Chem.* **1998**, *139*, 321. Kumada, N.; Takei, T.; Kinomura, N.; Wallez, G. *J. Solid State Chem.* **2006**, *179*, 793. Jiang, H.; Kumada, N.; Yonesaki, Y.; Takei, T.; Kinomura, N.; Yashima, M.; Azuma, M.; Oka, K.; Shimakawa, Y. *Jpn. J. Appl. Phys.* **2009**, *48*, 010216.

(24) Kinomura, N.; Kumada, N. *Mater. Res. Bull.* **1995**, *30*, 129.

up to 500 °C. Thermogravimetric analysis (TGA) and differential thermal analysis (DTA) was performed with a heating rate of 10 °C min^{-1} in either air or 3% H_2 in Ar using a Mettler-Toledo instrument.

Transmission electron microscopy was performed using either a JEOL 2000FX instrument or a JEOL 2100 LaB_6 instrument, both operating at 200 kV. The specimens were dispersed ultrasonically in ethanol and the deposited dropwise onto 3 mm lacey carbon grids supplied by Agar.

XANES experiments were performed using beamline B18 of the Diamond Light Source, U.K.[25] This beamline provides X-ray energies in the range 2.05−35 keV using a fixed-exit, double-crystal monochromator that holds two pair of crystals, Si (111) and Si (311). For this experiment the Si (111) pair was used, which provides an energy resolution of 2×10^{-4}. The optics of the beamline include a collimating mirror and a toroidal focusing mirror before and after the monochromator, respectively. The measurements presented here were carried out using the Cr coating of these two optical elements. A pair of harmonic rejection mirrors can also be used for measurements in the lower energy range. In this case, the Ni stripe of these mirrors was used for measurements at energies below 8 keV. Under this configuration, the expected flux on the sample is of the order of 5×10^{11} photons s^{-1} and the size of the beam at that position is approximately 200 μm in the vertical direction by 150 μm in the horizontal one. In our experiments, small samples (~20 mg) of materials to be studied were ground finely with polyethylene powder (~80 mg) under acetone and after evaporation of the solvent pressed into 13 mm diameter pellets of ~1 mm thickness under a pressure of 5 Tonnes. XANES data were collected at the Bi L_{III} and Ce L_{III} edges in transmission mode with ion chambers before and behind the sample filled with appropriate mixtures of inert gases to optimize sensitivity. The spectra were measured with a step size equivalent to less than 0.5 eV. Data were normalized using the program Athena[26] with a linear pre-edge and polynomial postedge background subtracted from the raw $\ln(I_t/I_0)$ data.

Total neutron scattering experiments were carried out using the instrument GEM[27] at ISIS, the U.K. spallation neutron source. The samples were loaded into vanadium cans with inner diameter 7.62 mm, and data were collected for approximately 5 h from each to ensure they were of good statistical quality. Data were also collected from an empty vanadium can, the empty instrument, and an 8.34 mm diameter vanadium rod for normalization purposes. The programs Gudrun[28] and ATLAS[29] were used to correct the data and produce the total-scattering structure factor, i(Q) (see the Supporting Information). The differential correlation function, D(r) was obtained by the standard approach[30] of Fourier transformation of i(Q), in this case with Q_{max} = 27 Å and using the Lorch modification function.[31] The function D(r) will hereafter be referred to as the pair distribution function (PDF). Rietveld refinement of the neutron scattering data was carried out on the data from the GEM detector bank 5 (mean scattering angle 91.42°) using the program GSAS,[32] and pair distribution function analysis was carried out using the program PDFgui.[33] PDFgui allows the refinement of a structural model with regard to real space (PDF) data, rather than reciprocal space (diffraction) data, by a method that is otherwise entirely analogous to the Rietveld method. Because the PDF contains information from both the Bragg and diffuse scattering and the real-space refinement is biased toward the local rather than long-range structure, PDF analysis is a method ideally suited to the study of nanocrystalline materials.

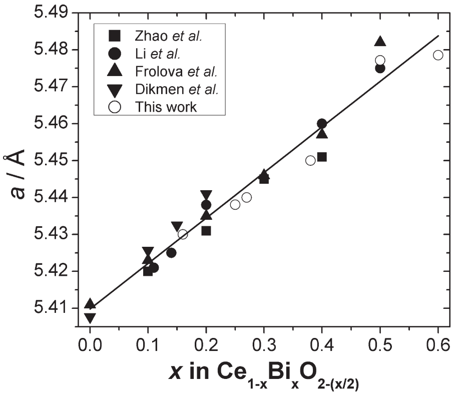

Figure 1. Lattice parameters of cerium−bismuth oxides. Literature data are taken from Zhao et al.,[20] Li et al.,[18] Frolova et al.,[22] and Dikmen et al.[17] The linear fit was obtained by linear regression (R^2 = 96%).

Temperature programmed reduction (TPR) experiments were performed at the Johnson Matthey Technology Centre, Sonning Common, Reading, U.K., using an in-house designed rig. The TPR experiments involved passing a 10% H_2 in N_2 gas mixture over the sample and measuring the thermal conductivity of the gas mixture after passing over the sample using a thermal conductivity detector. Initially a known amount of the gas mixture was injected into the system to act as a calibration peak in order to determine the amount of hydrogen consumed by the sample after the experiment. The sample was then heated at a rate of 10 °C min^{-1} to 773 K. The sample was then reoxidized using a temperature programmed oxidation (TPO) by a similar method but using a 10% O_2 in He gas mixture to 523 K. The data were analyzed by integration and comparison of the calibration peak to the sample peak.

Results and Discussion

1. Structure. Powder XRD indicated that the cerium−bismuth oxides are nanocrystalline, fluorite-type materials which exhibit lattice expansion with increasing Bi content and the profile is broadened considerably by the small particle size. Refined lattice parameters of six materials we have prepared are plotted in Figure 1, along with available data from materials with similar compositions reported previously by other groups. The elemental ratios used to define the composition of our samples were determined by a variety of methods: the results of elemental analysis for metals using ICP are contained in

---

(25) Dent, A. J.; Cibin, G.; Ramos, S.; Smith, A. D.; Scott, S. M.; Varandas, L.; Pearson, M. R.; Krumpa, N. A.; Jones, C. P.; Robbins, P. E. *J. Phys. Conf. Ser.* **2009**, *190*, 012039.

(26) Ravel, B.; Newville, M. *J. Synchrotron Radiat.* **2005**, *12*, 537.

(27) Williams, W. G.; Ibberson, R. M.; Day, P.; Enderby, J. E. *Phys. B* **1998**, *241−243*, 234. Hannon, A. C. *Nucl. Instrum. Methods Phys. Res., Sect. A* **2005**, *551*, 88.

(28) Soper, A. K.; Buchanan, P. Personal communication, **2004**.

(29) Hannon, A. C.; Howells, W. S.; Soper, A. K. *IOP Conf. Ser.* **1990**, *107*, 193.

(30) Wright, A. C. *Adv. Struct. Res. Diffr. Methods* **1974**, *5*, 1.

(31) Lorch, E. *J. Phys. C* **1969**, *2*, 229.

(32) Larson, A. C.; Dreele, R. B. V. Los Alamos National Laboratory Report LAUR 86-748, **1994**. Toby, B. H. *J. Appl. Crystallogr.* **2001**, *34*, 210.

(33) Farrow, C. L.; Juhas, P.; Liu, J. W.; Bryndin, D.; Bozin, E. S.; Bloch, J.; Proffen, T.; Billinge, S. J. L. *J. Phys.: Condens. Matter* **2007**, *19*, 335219.

Table 1. Compositional Information on Cerium−Bismuth Oxides Prepared by Hydrothermal Reaction Between $NaBiO_3 \cdot nH_2O$ and Ce^{3+}

sample	expected composition from reagent ratios		refined PDF composition[a]	refined Rietveld composition[a]	XRF	ICP
Ce75	Ce	0.75	0.82	0.77	0.78	0.76
	Bi	0.25	0.18	0.23	0.22	0.24
Ce50	Ce	0.5	0.46	0.65	0.65	0.52
	Bi	0.5	0.54	0.35	0.35	0.48
Ce40[b]	Ce	0.25	0.33	0.20	0.32	0.41
	Bi	0.75	0.67	0.80	0.68	0.59

[a] See Table 2 for errors on the refined values of composition. [b] The solid mixed-oxide product was manually separated from α-Bi_2O_3 byproduct (see text).

Table 1 for three representative compositions, and this also contains the refined compositions from the neutron scattering study which is described below. Note that using ICP only background levels of sodium could be detected in our samples. Reactions performed with molar Bi/Ce ratio of greater than 1.5 ($x > 0.6$) gave yellow powders of a mixed cerium−bismuth oxides along with larger crystals of α-Bi_2O_3 that could be physically separated (indeed in a control experiment in which Ce^{3+} is omitted from the reaction, only highly crysalline α-Bi_2O_3 is formed). The lattice parameter and elemental analysis data suggests a maximum Bi content in $Ce_{1-x}Bi_xO_y$ of $x = 0.6$ for the materials prepared using our synthetic route, and if a larger amount of Bi is used in the synthesis then phase separation occurs to give the $x = 0.6$ phase and α-Bi_2O_3. This limit is higher than seen in prevous work on cerium−bismuth oxides: for example, Dikmen et al. found a maximum of $x = 0.2$ for samples prepared from gels precipitated from Ce^{3+} and Bi^{3+} with ammonium hydroxide solution then heated at 260 °C.[17] Li et al. found a maximum $x = 0.5$ in samples prepared under hydrothermal conditions from Ce^{3+} and Bi^{3+} in NaOH solution at 240 °C,[18] and early work by Hund proposed that the solution limit was $x = 0.3$ for materials prepared using sintering at high temperatures.[34] It is possible, therefore, that the limit of doping in cerium−bismuth oxides is dependent on the method of synthesis. The expansion of the lattice parameter with increasing bismuth content is expected given the larger ionic radius of Bi^{3+}, but it should be noted that although δ-Bi_2O_3 is an oxygen deficient fluorite with $a = 5.6607$ Å,[35] it is only stable above 729 °C, therefore because of thermal expansion it is not possible to use as a room temperature pure bismuth end-member to compare with our materials. The linear relationship between lattice parameters and Bi content in doped ceria, seen in Figure 1 where we consider data from five independent studies, provide strong evidence for a solid-solution.

TEM analysis confirms the presence of small crystallites making up our samples, and Figure 2 shows some representative images that show the maximum particle dimension is around 10 nm. These images apparently show a dependence of particle size on composition, with the most Bi-rich materials showing smaller crystallites on average. The bulk, average particle size will be explored in more detail below when we discuss the neutron scattering results. Higher resolution TEM, Figure 3, reveals that the small crystallites show faceted surfaces: this illustrates the high crystallinity of individual particles.

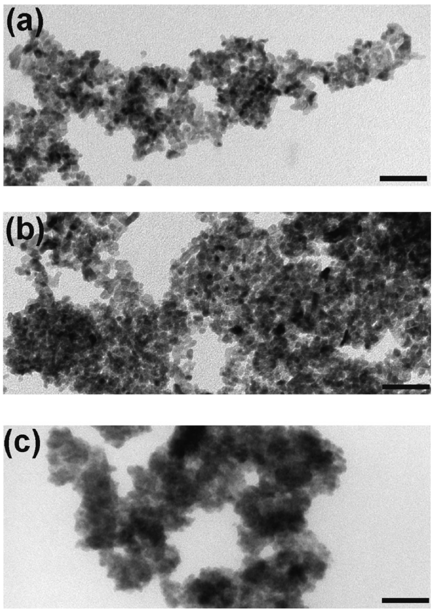

Figure 2. TEM images of three $Ce_{1-x}Bi_xO_{2-(x/2)}$ materials with (a) $x = 0.16$, (b) $x = 0.46$, and (c) $x = 0.60$. The scale bar in each case is 50 nm.

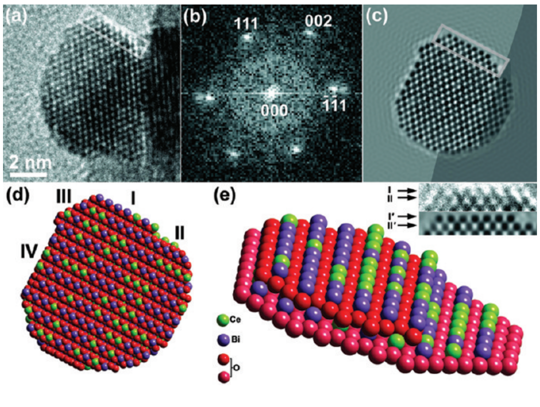

Figure 3. (a) High-resolution TEM image of a faceted crystallite of $Ce_{0.5}Bi_{0.5}O_{1.75}$ with one facet highlighted. (b) Indexed FFT obtained from the lattice image in part a. (c) A multislice image simulation produced for a similar fragment as in part a with the same facet highighted. (d) Faceted structure model used to produce the simulation in part c. I, II, III, and IV indicate (002), (002)′, (111), and (220) facets, respectively, assigned relative to part b. (e) Schematic surface structure model showing the (002) step and (002) terrace. Inset are details from the corresponding lattice image (i.e., I and II) and simulation (i.e., I′ and II′). Surface oxygens are omitted for clarity.

Figure 4 shows XANES spectra measured at the Bi L_{III} and Ce L_{III} edges. These spectra were recorded in order to

---

(34) Hund, F. *Z. Anorg. Allg. Chem.* **1964**, *333*, 248.
(35) Hull, S.; Norberg, S. T.; Tucker, M. G.; Eriksson, S. G.; Mohn, C. E.; Stolen, S. *Dalton Trans.* **2009**, 8737.

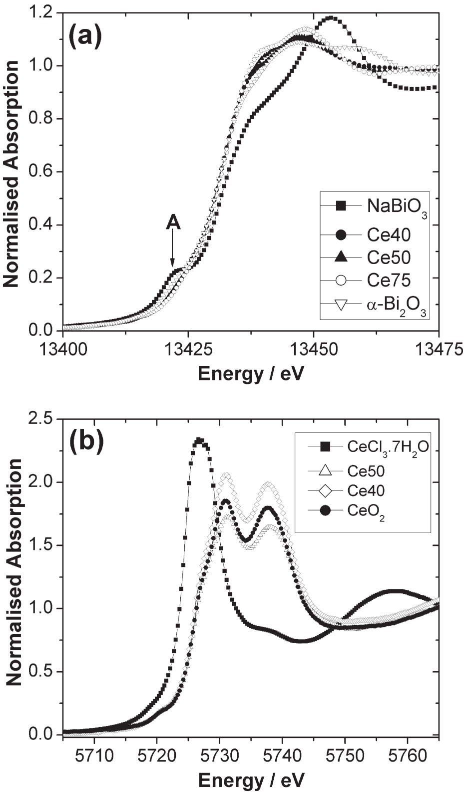

Figure 4. XANES spectra recorded at (a) the Bi L_{III}-edge and (b) the Ce L_{III}-edge. The labeling of the samples is defined in Table 1.

determine the oxidation state of the metals in the mixed oxides. This was important to establish since Kinomura and Kumada have shown that depending on reaction conditions the extent of reduction of $NaBiO_3 \cdot nH_2O$ varies to give either Bi^{5+} oxides, Bi^{3+} oxides, or mixed-valent materials.[24] Figure 4a shows clearly that bismuth is present as Bi^{3+} in the mixed cerium–bismuth oxides. The absence of a pre-edge peak (labeled A) shows that no Bi^{5+} remains in the mixed-metal oxides: this feature is clearly seen in $NaBiO_3 \cdot nH_2O$ and has previously been assigned to $2p^{3/2}$–6s transitions, since in the highest oxidation state the 6s orbital is unoccupied.[36] In addition, while there is a pronounced shift of the edge to higher energy for the higher oxidation state, the cerium–bismuth oxide materials show edge-shifts comparible to α-Bi_2O_3. It should also be noted at this point that although the XANES edge position of the mixed oxides is similar to α-Bi_2O_3, the form of the immediate postedge region shows some deviation: this suggests that the local atomic arrangement in the mixed oxides is different to that of bismuth in α-Bi_2O_3. The Ce L_{III}-edge XANES spectra show the presence of only Ce(IV) in the mixed cerium–bismuth oxides: the spectra show a distinctive double feature at a higher energy than the single white line seen in Ce(III) compounds, as has previously been discussed for other cerium-containing materials.[37] The complete reduction of the Bi(V) precursor and oxidation of the Ce(III) reagent is consistent with a chemical composition $Ce^{IV}{}_{1-x}Bi^{III}{}_{x}O_{2-(x/2)}$ ($x \leq 0.6$) for our materials.

Rietveld refinement against powder neutron diffraction data was performed using a fluorite type structure ($Fm\overline{3}m$) with statistical distribution of Ce and Bi over the eight coordinate metal site, Figure 5, gives cubic lattice parameters and compositional information. Because of the broadness of the peaks, it was not possible to refine independently all of the occupancies and thermal displacement parameters. Therefore a charge-balancing constraint was applied (such that an increase in Bi content would be matched by a proportional decrease in O content) to reduce the total number of parameters refined. Table 2 contains the refined crystal parameters and goodness of fit indices.

An estimation of nanoparticle diameter is possible from a PDF by considering the decay of the function at high r,[38] and Figure 6 shows the PDFs for the three samples studied by total neutron scattering. Although this damping also has contributions from the instrument resolution,[39] the Q range used in the Fourier transform,[31] and the influence of thermal motion,[40] a trend of decreasing particle size with increased bismuth content is clearly visible. The general trend is not only consistent with the TEM images presented above, but the approximate values of crystal diameters derived are physically reasonable and compare well between the two techniques.

A full analysis of the PDFs was used to compare the two potential structural models: a fluorite-type solid-solution model and a mixed-phase model (either a binary mixture of CeO_2 and α-Bi_2O_3 or of CeO_2 and β-Bi_2O_3). For all three compositions, the mixed phase models gave poor agreement with the experimental PDF, particularly at $r > 5$ Å (see the Supporting Information). The solid-solution model provided an excellent overall fit and refined structural parameters in good agreement with those from Rietveld analysis (Figure 7 and Table 2). On closer inspection, however, the relatively poor fit to the first two peaks (corresponding to the nearest-neighbor M–O and O–O distances, respectively) indicated significant local distortion. Hull et al. have recently examined the structure of δ-Bi_2O_3 using neutron total scattering and reverse Monte Carlo (RMC) simulations and found that although the average structure could be assigned to a cubic fluorite structure, the local coordination environment of the Bi closely resembled that of the tetragonal polymorph β-Bi_2O_3.[35] Since the structure of β-Bi_2O_3 is

---

(36) Heald, S. M.; Dimarzio, D.; Croft, M.; Hegde, M. S.; Li, S.; Greenblatt, M. *Phys. Rev. B* **1989**, *40*, 8828. Guyot, H.; Filippini, C.; Marcus, J. *J. Alloys Compd.* **1993**, *195*, 543. Demourgues, A.; Dussarrat, C.; Bontchev, R.; Darriet, B.; Weill, F.; Darriet, J. *Nucl. Instrum. Methods Phys. Res., Sect. B* **1995**, *97*, 82. Mizoguchi, H.; Hosono, H.; Kawazoe, H.; Yasukawa, M.; Fujitsu, S.; Fukumi, K. *Mater. Res. Bull.* **1999**, *34*, 373. Jiang, N.; Spence, J. C. H. *J. Phys.: Condens. Matter* **2006**, *18*, 8029.

(37) Takahashi, Y.; Sakami, H.; Nomura, M. *Anal. Chim. Acta* **2002**, *468*, 345. Modeshia, D. R.; Wright, C. S.; Payne, J. L.; Sankar, G.; Fiddy, S. G.; Walton, R. I. *J. Phys. Chem. C* **2007**, *111*, 14035.

(38) Jolley, C. C.; Uchida, M.; Reichhardt, C.; Harrington, R.; Kang, S.; Klem, M. T.; Parise, J. B.; Douglas, T. *Chem. Mater.* **2010**, *22*, 4612.

(39) Grimley, D. I.; Wright, A. C.; Sinclair, R. N. *J. Non-Cryst. Solids* **1990**, *119*, 49.

(40) Parker, S. F.; Refson, K.; Hannon, A. C.; Barney, E. R.; Robertson, S. J.; Albers, P. *J. Phys. Chem. C* **2010**, *114*, 14164.

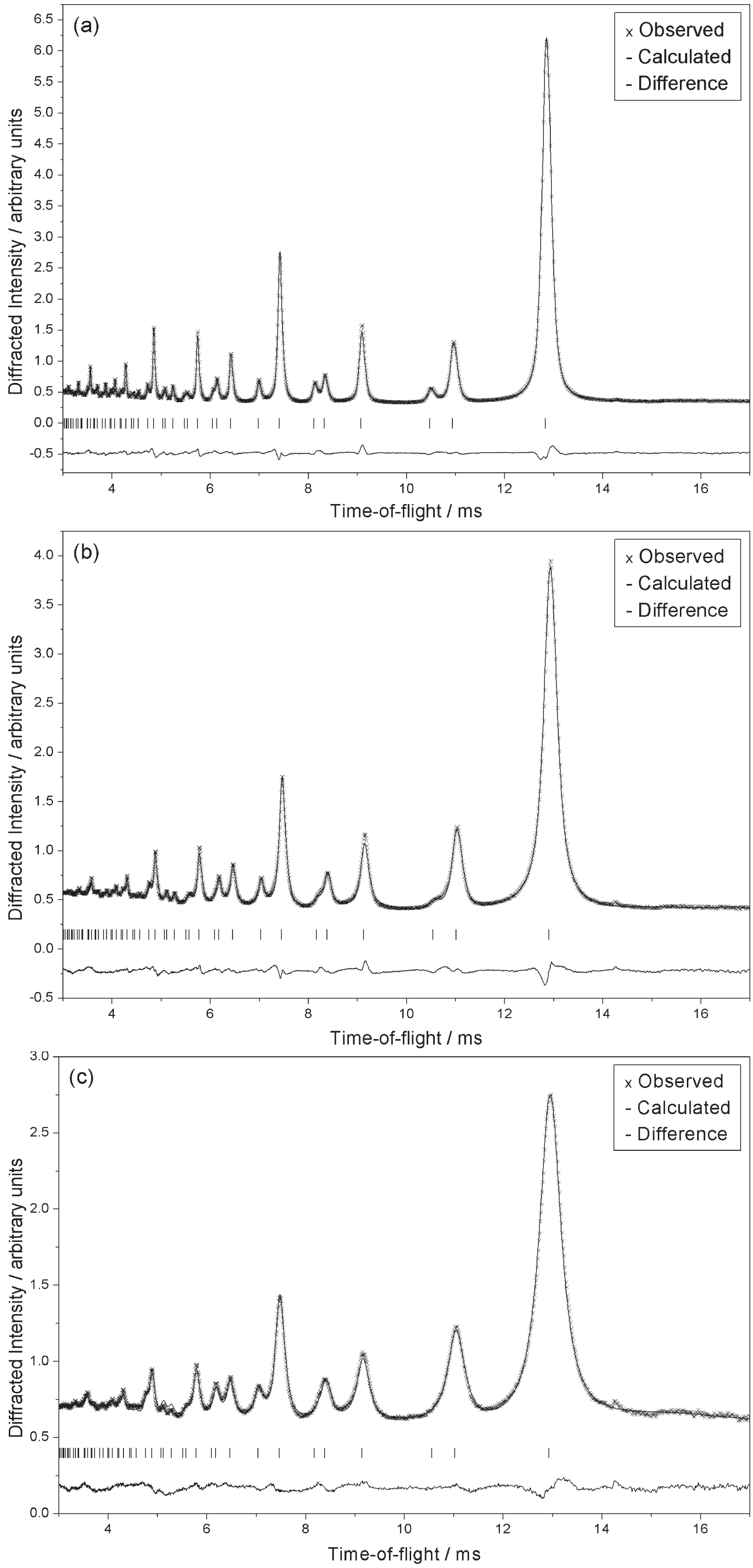

Figure 5. Fits to the powder neutron diffraction data using the Rietveld method for $Ce_{1-x}Bi_xO_{2-(x/2)}$ with (a) $x = 0.25$, (b) $x = 0.5$, and (c) $x = 0.6$. See Table 2 for refined crystal parameters. The tick marks denote the positions of Bragg peaks for the $Fm\bar{3}m$ fluorite unit cell.

closely related to the fluorite structure, this was considered an appealing model for the local structure of our solid solutions. The first two peaks in the PDFs were then fitted successfully with a mixture of CeO_2 and β-Bi_2O_3 (Figure 7, insets). The local structure of the Bi in each of our materials then is described well as a distorted square-pyramidal

Table 2. Refined Crystal Structure Parameters for Cerium−Bismuth Oxides from Rietveld and PDF analysis of Neutron Diffraction Data

sample	Ce75		Ce50		Ce40	
	Rietveld	PDF	Rietveld	PDF	Rietveld	PDF
a/Å	5.4380 (7)	5.4390 (2)	5.4771 (1)	5.4682 (4)	5.4786 (2)	5.4801 (1)
Occ. Ce	0.773 (7)	0.800 (1)	0.65 (1)	0.457 (2)	0.206 (7)	0.334 (4)
Occ. Bi	0.227 (7)	0.200 (1)	0.35 (1)	0.543 (2)	0.794 (7)	0.666 (4)
Occ. O	0.943 (7)	0.950 (1)	0.913 (1)	0.864 (2)	0.802 (7)	0.834 (4)
U_{iso} (Ce/Bi)/Å^2	0.0071 (3)	0.008 85 (2)	0.0081 (5)	0.016 02 (5)	0.0116 (2)	0.014 48 (8)
U_{iso} (O)/Å^2	0.0099 (2)	0.012 98 (1)	0.0179 (6)	0.018 65 (4)	0.0194 (3)	0.020 07 (9)
R_{wp}	0.0328	0.169	0.0303	0.263	0.0226	0.265
R_{p}	0.0231		0.0233		0.0203	
spdiameter/Å^a		114		71		42

^{a} spdiameter is an estimation of particle size from the PDFgui program based on a convolution of the ideal PDF (given the experimental conditions under which the data were measured and the range of Q used for Fourier transformation) for an infinite lattice and a spherical shape function.

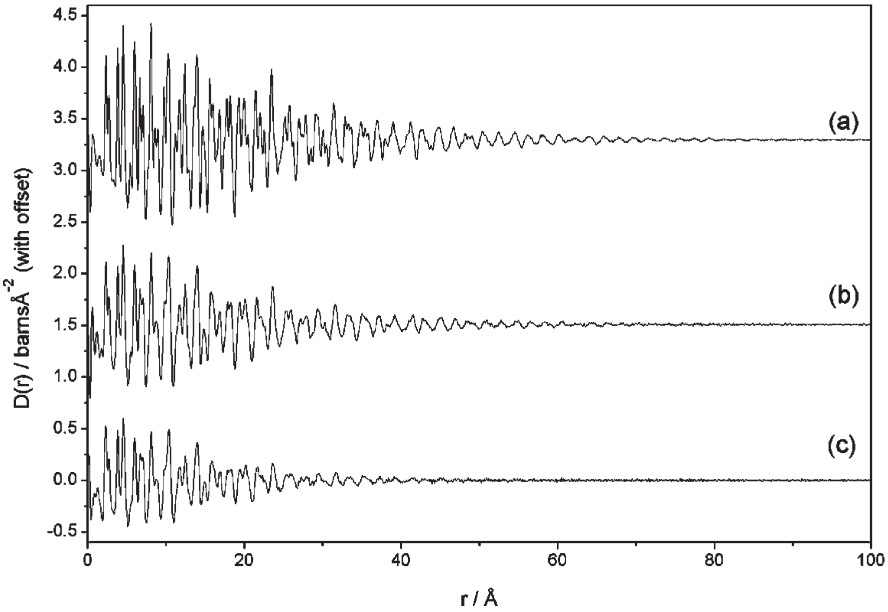

Figure 6. PDFs derived from total neutron scattering for $Ce_{1-x}Bi_xO_{2-(x/2)}$ with (a) $x = 0.25$, (b) $x = 0.5$, and (c) $x = 0.6$.

arrangement of oxygen atoms with bond lengths ranging from 2.17 to 2.87 Å; these values are in good agreement with those for β-Bi_2O_3.[41] Furthermore, the distribution of O−Bi−O bond angles also matches well (see the Supporting Information).

2. Thermal and Redox Properties. Figure 8 shows temperature programmed reduction plots under hydrogen flow for three representative materials (see the Supporting Information for more examples and full analysis). These all show a large hydrogen uptake at around 600 K. This reduction appears to be reversible, since after mild oxidation in dilute oxygen, a second TPR (performed immediately *in situ*) shows reduction at similar temperatures, also shown in Figure 8. TPR has been widely used as a diagnostic test of redox properties of ceria and doped ceria materials for a good many years, and there are many literature reports of standard results for such systems.[42,43] For high surface area ceria it is expected that reduction of surface cerium gives a feature at around 650 K, which is followed by bulk reduction at > 1100 K upon continued heating.[44] The ratio of the areas of these surface and bulk reduction features depends then on the crystallite size of the ceria. The reduction of ceria takes place at considerably lower temperature if used as a support for a precious metal,[43] and in doped ceria-based materials, low temperature reduction in TPR is commonly observed: this has been particularly well-documented in the case of ceria-zirconia materials[7] but is also seen also in other doped systems.[11,45] Blank et al. made a detailed study of ceria doped with 10% of a variety of metals, including bismuth, and found that the most obvious change in the TPR, compared to pure ceria, was the lowering of the onset of low temperature reduction, which was ascribed to dissociative adsorption of hydrogen being the rate determining step.[46] They also noted that surface activity alone is not responsible for low temperature reduction but

---

(41) Blower, S. K.; Greaves, C. *Acta Crystallogr., Sect. C: Cryst. Struct. Commun.* **1988**, *44*, 587.

(42) Yao, H. C.; Yao, Y. F. Y. *J. Catal.* **1984**, *86*, 254. Bernal, S.; Blanco, G.; Calvino, J. J.; Gatica, J. M.; Omil, J. A. P.; Pintado, J. M. *Top. Catal.* **2004**, *28*, 31.

(43) Boaro, M.; Vicario, M.; Leitenburg, C. d.; Dolcetti, G.; Trovarelli, A. *Catal. Today* **2003**, *77*, 407.

(44) Perrichon, V.; Laachir, A.; Bergeret, G.; Frety, R.; Tournayan, L.; Touret, O. *J. Chem. Faraday Trans.* **1994**, *90*, 773.

(45) Singh, P.; Hegde, M. S. *Cryst. Growth Des.* **2010**, *10*, 2995.

(46) Blank, J. H.; Beckers, J.; Collignon, P. F.; Rothenberg, G. *ChemPhysChem* **2007**, *8*, 2490.

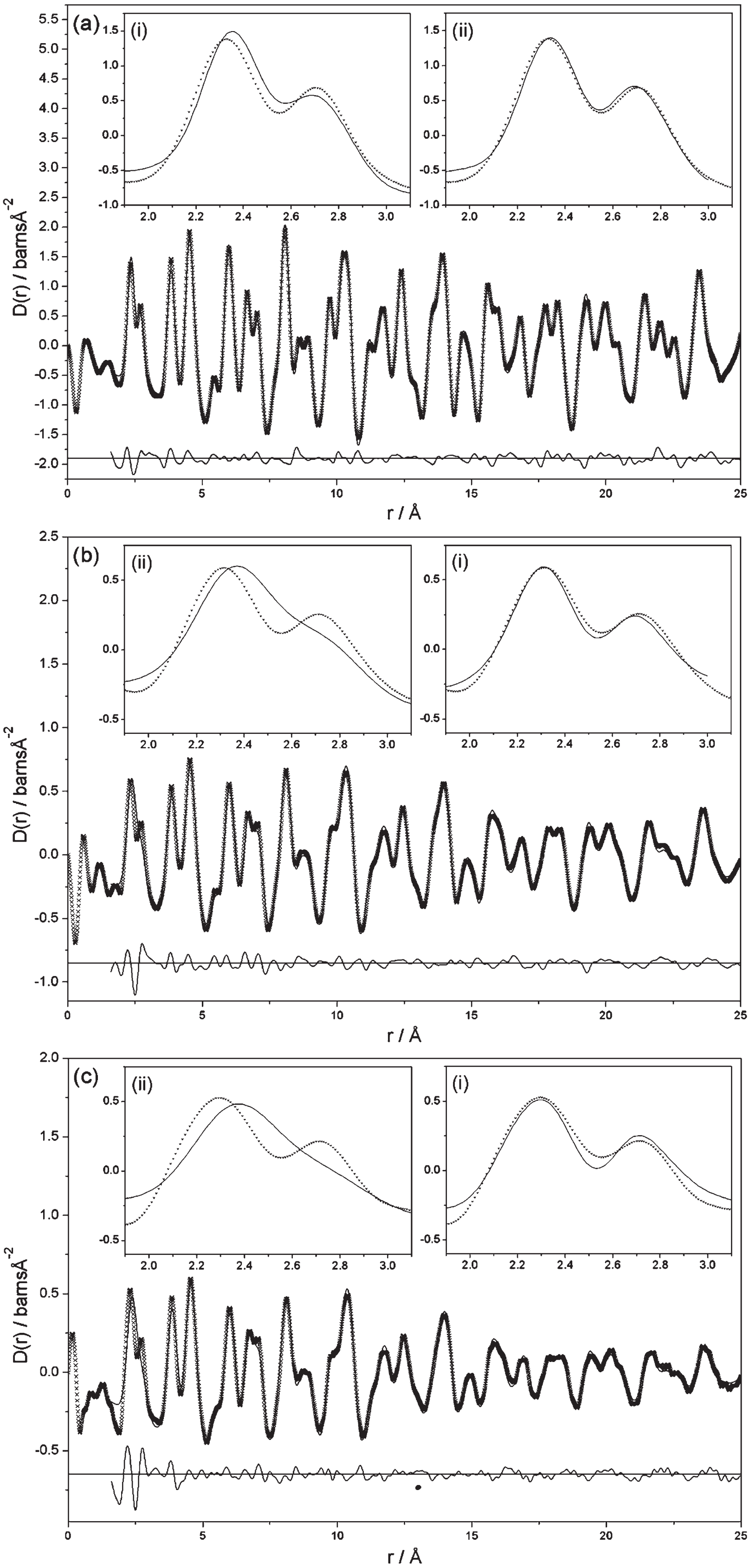

Figure 7. Fits to the PDFs for $Ce_{1-x}Bi_xO_{2-(x/2)}$ with (a) $x = 0.25$, (b) $x = 0.5$, and (c) $x = 0.6$. The insets labeled (i) and (ii) correspond to the fits to the local structure as average fluorite model and a model in which the bismuth is present in an environment like in β-Bi_2O_3, respectively.

that the nature of the metal added was also important for defining the redox activity. Thus, for our cerium−bismuth oxides it is not unexpected that significant reduction takes place below 650 K, where the presence of bismuth in a distorted coordination environment, an expanded lattice compared to CeO_2, and also oxide ion vacancies to balance the lower charge of bismuth would all point toward greater oxide ion mobility. Further analysis of the TPR data was performed by peak deconvolution to determine the areas and positions of the main reduction features, Table 3.

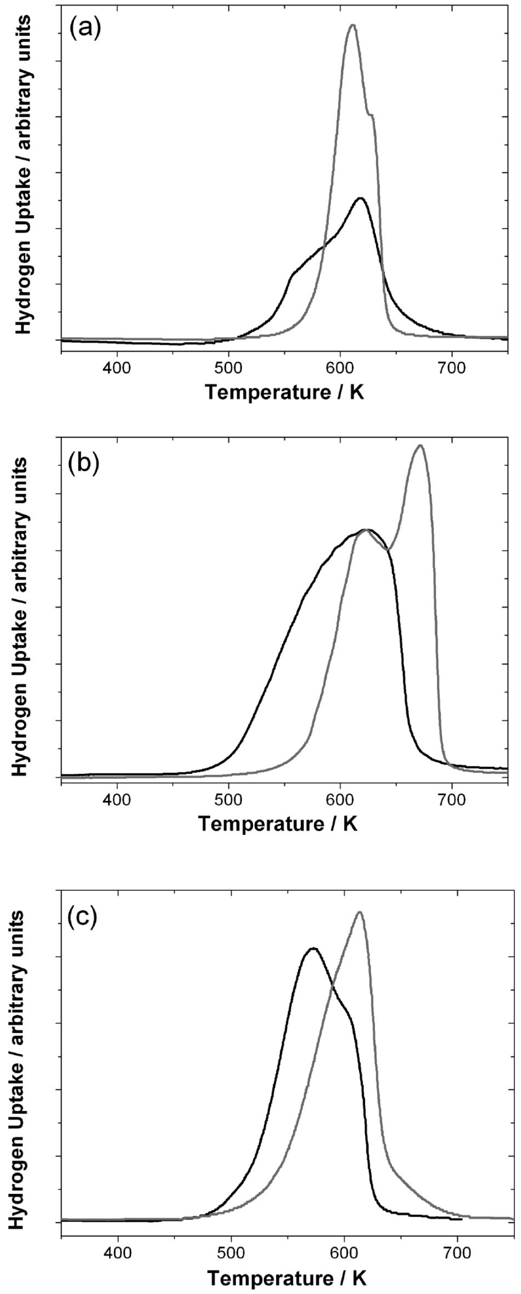

Figure 8. TPR traces for three cerium−bismuth oxides $Ce_{1-x}Bi_xO_{2-(x/2)}$ with (a) $x = 0.25$, (b) $x = 0.5$, and (c) $x = 0.6$. The black trace is the first TPR and the gray trace the second (after an intermediate reoxidation).

The amount of H_2 taken up in each TPR run is plotted in Figure 9: this shows an increase in hydrogen uptake with bismuth content, which may be correlated to the greater distortion of the ideal fluorite structure with increasing dopant and certainly matches the expansion of the fluorite lattice (Figure 1). Complementary thermogravimetric analysis in air and under dilute hydrogen flow, Figure 10, also confirms a significantly high percentage of total mass loss (up to ∼14.5%) under H_2 gas atmosphere compared to that in air (up to 4.5%) in all bismuth doped ceria samples, and furthermore the percentage mass loss varies with increasing bismuth content

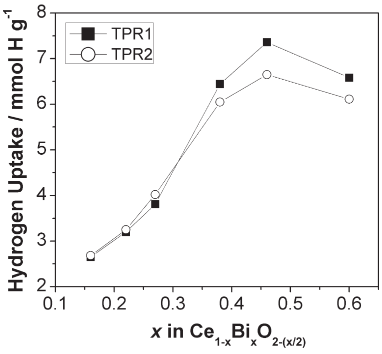

Figure 9. Analysis of TPR data showing hydrogen uptake vs bismuth content in $Ce_{1-x}Bi_xO_{2-(x/2)}$.

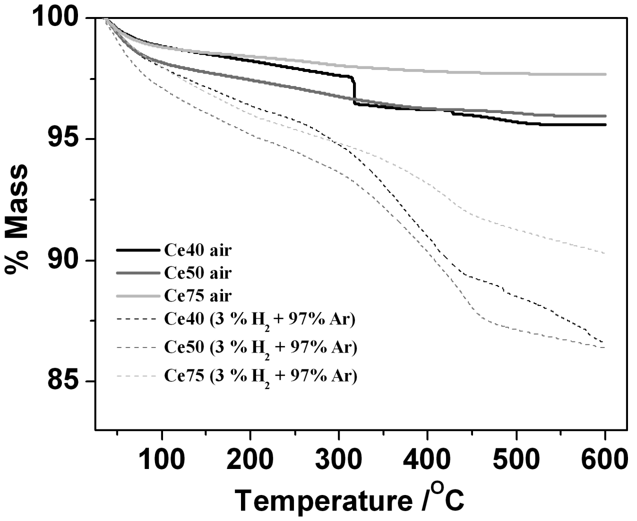

Figure 10. TGA traces for three $Ce_{1-x}Bi_xO_{2-(x/2)}$ samples under two different gas atmospheres (see Table 1 for sample descriptions).

Table 3. Summary of Results of Temperature Programmed Reduction Experiments on Cerium−Bismuth Oxides

composition: x in $Ce_{1-x}Bi_xO_{2-(x/2)}$	mmol of Ce g $^{-1a}$	hydrogen uptake TPR1/mmol H g $^{-1}$	temperature of majority of TPR1/K	hydrogen uptake TPR2/mmol H g $^{-1}$	temperature of majority of TPR2/K
0.16	4.62	2.65	349.0	2.68	344.0
0.22	4.20	3.2	344.1	3.25	339.4
0.27	3.87	3.81	329.8	4.02	292.9
0.38	3.18	6.44	346.1	6.05	331.6
0.46	2.70	7.36	314.9	6.65	353.3
0.6	1.92	6.58	297.9	6.11	327.8

[a] Calculated from the chemical formula in the preceding column.

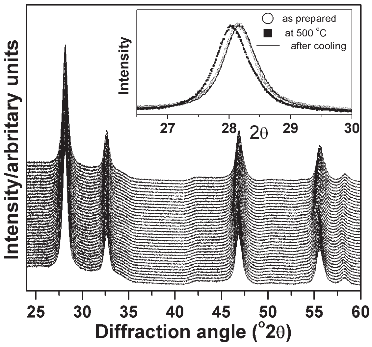

Figure 11. *In situ* powder XRD patterns of $Ce_{0.5}Bi_{0.5}O_{1.75}$ recorded upon heating in air. The figure contains diffractograms recorded at temperatures on heating from 50 to 500 then on cooling to 50 °C with an interval of 25 °C bottom to top, respectively. All patterns are equally offset along the y axis for clarity. The inset shows enlarged view of fluorite (111) peak recorded at 30 °C and after heating up to 500 °C along with the one recorded at 500 °C, the latter showing temperature induced lattice expansion but no peak sharpening.

in the same way as the hydrogen uptake seen by TPR. In air, mass loss of around 4.5% (with a broad, featureless DTA trace) may be attributed to the removal of surface adsorbed species, such as water or hydroxide, so the additional loss under reductive conditions must be due to loss of oxygen from the solids. A closer examination of the hydrogen uptake and TGA data, however, reveals that the values correspond to significantly more than reduction of just Ce^{4+} to Ce^{3+}; this is particularly apparent in the highest bismuth-containing materials, as shown in Table 2. In fact, for CeO_2 itself it is not possible to reduce completely to Ce_2O_3 without heating under a flow of pure hydrogen at 1000 °C,[47] so reduction of all the cerium in ceria under the mild TPR condition is not expected. This immediately suggests that the apparent reversibility of the reduction of the cerium−bismuth oxides is more complex and involves more than just reduction of Ce^{4+}.

XRD under air flow on heating to 500 °C shows no evidence for annealing of the crystallites, with no detectable change in Bragg peak widths, Figure 11. Under H_2 flow (5% in nitrogen; more dilute than in the TPR experiment), clear phase separation to Bi metal[48] is seen by *in situ* XRD, Figure 12a. It should be noted that the apparent disappearence of bismuth above 200 °C does not indicate the reincorporation of bismuth into the ceria lattice, but these correspond to the melting of bismuth metal (melting point 270 °C). The large H_2 uptake we see in TPR is explained by the extrusion of Bi_2O_3 from the mixed oxide and its reduction to bismuth metal. Even after an oxidation step (heating in air to 500 °C), Bi metal is still present, Figure 12b, and there is no sign of crystalline Bi_2O_3. The "reversibility" we observe in the TPR experiment therefore is not due to reoxidation of bismuth metal to Bi_2O_3 (or indeed to $Ce_{1-x}Bi_xO_{2-(x/2)}$ with re-incorporation of bismuth) with subsequent reduction but due to the fact that in the first TPR cycle not all the Bi has been extruded from the mixed oxide. It takes several cycles before all the Bi is removed from $Ce_{1-x}Bi_xO_{2-(x/2)}$ and therefore TPR appears to be reversible over several cyles. Evidence for the model comes from XRD recorded after each of three TPR cycles, where a gradual decrease of lattice parameter toward the value expected for CeO_2 is seen (Supporting Information). This is further proved by examining a sample of $Ce_{0.5}Bi_{0.5}O_{1.75}$ that has been treated to three reduction cycles *ex situ*: SAED in the TEM, Figure 13, shows the presence of both fluorite-like mixed oxide and is also evidence for phase-separated, finely divided bismuth metal, a material that is rather beam sensitive. The TPR of a material pre reduced with six cycles of hydrogen flow and air oxidation shows considerably lower hydrogen uptake than a pristine sample (Supporting Information).

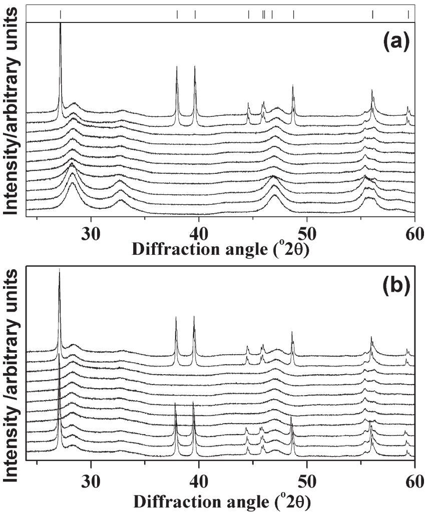

Figure 12. *In situ* powder XRD pattern of $Ce_{0.5}Bi_{0.5}O_{1.75}$ recorded during heating from 30 to 500 to 30 °C from top to bottom (a) with an as-prepared sample, heated in under 5% H_2 and (b) with a reduced sample heated in air atmosphere. The upper panel in part a shows the tick marks expected for rhombohedral bismuth metal (a = 4.546 Å and c = 11.862 Å)[48] In both parts a and b, the first and last diffractograms correspond to a temperature of 30 °C while second onward are within 100−500−100 °C with an interval of 100 °C.

Conclusions

We have presented a comprehensive study of some new samples of cerium−bismuth oxides using a variety of techniques. The structural and spectroscopic studies allow us to describe the series of materials as Ce^{IV}_{1-x}-$Bi^{III}_{x}O_{2-(x/2)}$ ($x \leq 0.6$) with the long-range structure of the fluorite lattice but with local distortion due to the asymmetric coordination preference of Bi(III). A larger amount of bismuth can be introduced using mild hydrothermal conditions, compared to other reported synthetic approaches. While previous work on cerium−bismuth oxides has reported high oxide ion mobility in samples sintered at high temperatures in air, we have focused on an examination of redox properties using TPR under dilute hydrogen as a standard test of redox behavior in catalyst supports. For $Ce^{IV}_{1-x}Bi^{III}_{x}O_{2-(x/2)}$ large hydrogen uptakes at temperatures lower than for CeO_2 itself

---

[47] Wetzel, K. In *Handbook of Preparative Inorganic Chemistry*; Brauer, G., Ed.; Academic Press: New York, 1965; Vol. *2*, p 1151.

[48] Cucka, P.; Barrett, C. S. *Acta Crystallogr.* **1962**, *15*, 865.

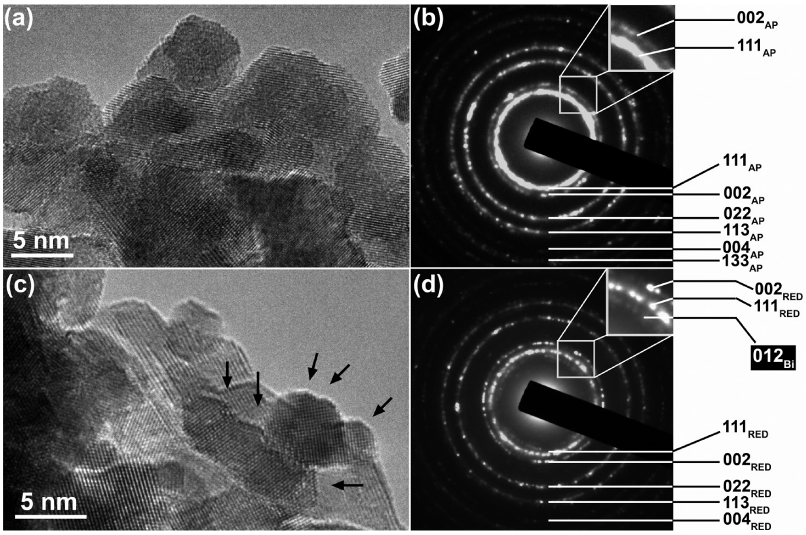

Figure 13. High-resolution TEM image of $Ce_{0.5}Bi_{0.5}O_{1.75}$ (a) before ("as-prepared") and (c) after reduction (three TPR cycles), along with indexed SAED patterns in parts b and d, respectively. The labels AP and RED denote as-prepared and reduced, respectively, and the diffraction ring due to rhombohedral bismuth is denoted Bi. Extensive faceting is visible in the main image (arrowed).

reflect the fact that the cerium−bismuth oxides undergo phase separation to yield bismuth metal and more cerium rich oxides. This suggests that while the nanocrystalline cerium−bismuth oxides are not suited for use under reducing conditions at elevated temperature, given their stability toward annealing in air, they may still have desirable applications in milder oxidation catalysis.

Acknowledgment. We thank the EPSRC for funding this work (Grant EP/F012721). Some of the equipment used in materials characterisation at the University of Warwick was obtained through the Science City Advanced Materials project "Creating and Characterising Next Generation Advanced Materials" with support from Advantage West Midlands (AWM) and part funded by the European Regional Development Fund (ERDF). We are grateful to the STFC for provision of beamtime at ISIS and at Diamond and for part-funding a studentship for H.Y.P. via its Centre for Materials Physics and Chemistry. We thank Steve York (Warwick) for some preliminary TEM work.

Supporting Information Available: PDF analysis of neutron scattering data, temperature programmed reduction, powder XRD of reduced samples, and TPR of reduced sample (PDF). This material is available free of charge via the Internet at http://pubs.acs.org.